Plasma enhanced atomic layer deposition of a (nitrogen doped) Ti phosphate coating for improved energy storage in Li-ion batteries

Peer-reviewed author version

Henderick, Lowie; HAMED, Hamid; Mattelaer, Felix; Minjauw, Matthias; Meersschaut, Johan; Dendooven, Jolien; SAFARI, Momo; Vereecken, Philippe & Detavernier, Christophe (2021) Plasma enhanced atomic layer deposition of a (nitrogen doped) Ti phosphate coating for improved energy storage in Li-ion batteries. In: JOURNAL OF POWER SOURCES, 497 (Art N° 229866).

DOI: 10.1016/j.jpowsour.2021.229866
Handle: http://hdl.handle.net/1942/33898

PE-ALD of N-doped Ti-phosphate for improved energy storage in Lithium ion batteries

Lowie Henderick,[†] Hamid Hamed,[‡,¶] Felix Mattelaer,[†] Matthias Minjauw,[†] Johan Meersschaut,[§] Jolien Dendooven,[†] Mohammadhosein Safari,[‡,¶,‖] Philippe Vereecken,[§] and Christophe Detavernier*[,†]

†*Department of Solid State Sciences, Ghent University, Krijgslaan 281 S1, 9000 Gent, Belgium*

‡*UHasselt, Hasselt University,Institute for material research (IMO), 3590 Diepenbeek, Belgium*

¶*EnergyVille 2, Thor park 8320, 3600 Genk, Belgium*

§*imec, Kapeldreef 75, B-3001 Heverlee, Belgium*

‖*IMEC division IMOMEC, BE-3590, Belgium*

E-mail: Christophe.Detavernier@Ugent.be

Abstract

PE-ALD of nitrogen doped Ti-phosphate has been investigated in two different deposition processes. Both processes were analysed by in-situ ellipsometry (to monitor the growth of the film) and X-ray photoelectron spectroscopy/elastic recoil detection (to study the composition). First, previous knowledge on rapid PE-ALD of undoped Ti-phosphate using an exposure sequence of trimethyl phosphate plasma - oxygen plasma - titanium isopropoxide, i.e. TMP* - O^*_2 - TTIP, was used to

test an altered process using a nitrogen plasma, i.e. TMP* - N^*_2 - TTIP. This process enabled the deposition of a nitrogen doped (6 at.%) Ti-phosphate with a growth per cycle of 0.4 nm/cycle. Next, a dual-source precursor (diethyl phosphoramidate plasma, or DEPA*) was introduced instead of TMP*, incorporating both nitrogen and phosphorus. This allowed for a higher growth rate (0.6 nm/cycle) and a higher nitrogen level (8.6 at.%). To study the effect of nitrogen doping on the electrochemical performance of Ti-phosphate as a coating material, the thin film resulting from the latter deposition process was electrochemically compared to undoped Ti-phosphate. It was found that the ionic transparency of the coating has slightly decreased due to nitrogen doping, but the electronic conductivity significantly increased. When a lithium nickel manganese cobalt oxide powder based electrode (NMC) is coated with 2 nm of (un)doped Ti-phosphate, a significant improvement in the rate capability is found for both coatings, without harming the capacity retention.

Introduction

In the investigation towards improved energy storage in Li-ion battery's (LIB), altering the cathode surface by the deposition of a thin coating layer has proven to be very successful. It has for example been shown that the deposition of materials that are typically inactive towards reactions with Li-ions[1], and have a low electronic conductivity, can improve the cycling stability of the electrode. This is because of the physical barrier that materials such as Al_2O_3[2] and Al-phosphate[3-7] impose, inhibiting parasitic reactions that are detrimental to the cycling stability. The down side of the inert nature of these coatings is however that poor ionic and/or electronic conductivity will decrease the amount of energy that can be stored in the electrode, especially at higher current densities[8,9]. In other words, the amount of energy that can be stored in the electrode is sacrificed (by means of a increase in ionic and electronic resistance at the particle surface) for improved cycling stability.

For powder-based electrodes, the poor electronic conductivity can be tackled by coating the electrode sheet, instead of the electrode particles[10]. This will allow for protection against

parasitic reactions without breaking the contact between the carbon black and the electrode particle. However, this technique limits the amount of materials that can be deposited, as the binder that is used in these electrode sheets is typically not stable at elevated temperatures.

In tackling the poor ionic conductivity (important for both thin film and powder based electrodes), the coating has to be very thin so that it is made transparent to Li-ions. However, even at the sub-nanometer scale, these coatings will decrease the amount of energy stored in the electrode at high current densities[8]. Next to this, the need for ultra-thin coatings demands a very high control over thin film thickness, as the slightest amount of uncontrolled growth will be detrimental for the electrode's capacity.

In order to avoid all of these problems, further increasing the battery performance, alternative options have to be investigated. One option is to alter the existing inert coating materials, in order to increase their ionic and/or electronic conductivity. Nitrogen doping of Al-phosphate has for example significantly improved the electrochemical performance of the coating, allowing for an enhancement of the electrode's rate capability[9]. Another option is to step away from these inert materials, and start looking at materials that have shown to be electrochemically active (at a potential that differs from the material on which it can be coated). Due to this electrochemically active nature of the coating, smooth transportation of Li-ions and electrons is expected, allowing for good rate capability. This has proven to be a valid alternative in the work of Xiao et al., in which an Fe-phosphate coating on LNMO showed improved cyclability and improved storage at high current densities[11]. Using such an electrochemically active material as a coating[11,12] could thus not only lead to an increase in the ionic and electronic conductivity at the electrolyte-electrode interface, but also decrease the need for a highly controlled coating thickness (as there is no need for ultra-thin films).

If this coating needs to be deposited on a complex surface, such as electrode particles,

Atomic Layer Deposition (ALD) is a very interesting deposition technique[13]. This technique uses a series of reactions of gaseous precursors with the substrate, to grow the layer of interest. This is similar to Chemical Vapour Deposition (CVD), but is more controlled due to the self-limiting behaviour of the reactions (within a specific ALD temperature window). Because of this self-limitation, one layer of the desired coating is deposited per cycle, allowing for the growth of highly conformal and pinhole free layers. In most ALD processes, thermal reactions are used. However, including a plasma (plasma-enhanced ALD, or PE-ALD) can allow for a higher reactivity, enabling growth of materials that are not possible otherwise.

Over the last couple of years, using ALD to deposit different kinds of phosphates has gained more and more interest. The high stability of the strong P-O bonds allow for example the use of a variety of phosphates in Li-ion battery (LIB) applications, ranging from protective coatings (Al-phosphate[3–6]) to cathode materials[14] (Fe-phosphate[15], Ti-phosphate[16]). Recently, Dobbelaere et al. introduced a PE-ALD process that allowed for fast deposition of an Al-phosphate using a combination of Trimethyl phosphate plasma (TMP*) with an oxygen plasma and trimethylaluminum (TMA). In changing the last process step into a different metal precursor, deposition of titanium[16], vanadium[18], zinc[19], iron[15] and cobalt phosphate[20] became possible.

A lot of research on titanium phosphate in particular is typically based on its interesting ion-exchange properties and its catalytic activity. Besides this, both current generation Li-ion batteries[16,21] (LIB) and next generation Sodium ion batteries[22] (SIB) make use of its high structural and thermal stability to use it as a positive electrode material. However, Ti-phosphate also perfectly fits in the framework of using an electrochemically active material as a coating for LIB electrodes. Due to its ability to store Li-ions, the ionic and electronic resistivity at the coating interface is expected to be significantly lower than with the standard inert coatings (such as Al_2O_3[8] and Al-phosphate[9]), improving the battery performance.

As even electrochemically active phosphates still suffer from a relatively poor electronic conductivity[17], their electrochemical performance could possibly be enhanced even more. Nb-doping has for example been shown to result in improved electrochemical behaviour when using Ti-phosphate as a battery electrode[23], opening up different ways to improve the electrochemical properties of the material. In this work, altering the electrochemical properties through nitrogen doping will be investigated[9,24,25], in line with our recent work on nitrogen doped Al-phosphate[9]. In that work, PE-ALD of nitrogen doped aluminium phosphate was be obtained by combining a diethyl phosphoramidate plasma (DEPA*, where the star denotes plasma) or Trimethyl phosphate plasma (TMP*) with nitrogen plasma and trimethylaluminum (TMA)[9]. It was found that through this nitrogen doping, the electronic conductivity of the Al-phosphate significantly increased. However, it is not known if this deposition process can easily be transferred from one type of phosphate (e.g. Al-phosphate, by using TMA) to another (e.g. Ti-phosphate, by using TTIP).

In this work, a strategy similar to our recent work on nitrogen doping of Al-phosphate will be used to study the deposition of nitrogen doped Ti-phosphate, in an attempt to improve its electrochemical properties. Two different ways of nitrogen doping will be investigated and the most nitrogen rich material will be electrochemically characterised (and compared to undoped Ti-phosphate) as a LIB electrode coating.

Experimental section

Deposition system. A home-built high-vacuum ALD system with a base pressure of approximately $5 * 10^{-6}$ mbar was used to deposit the films, for which the reactor design is very similar to the system used in the work by Dobbelaere et al.[15] To reach this base pressure, the reactor walls were heated up to 120 °C and the chamber was pumped with a turbomolecular pump. The TMP

(Sigma-Aldrich, 97%) and TTIP (Sigma-Aldrich, 97%) precursor bottles were heated up to 45 °C and 60 °C, while manually adjustable needle valves were installed to control the pressure of nitrogen gas and oxygen gas at a value of approximately $5 * 10^{-3}$ mbar. DEPA (Sigma-Aldrich, 98%) was heated up to 115 °C, and its vapour was introduced in the reactor using argon at a pressure of $5 * 10^{-3}$ mbar as carrier gas. The plasma power was selected to be 200 W for nitrogen gas, TMP and DEPA, while the oxygen gas was pulsed as a 300 W plasma. The plasma was delivered to the sample surface using a remote ICP-RF plasma located above the sample surface.

Material characterization. In situ spectroscopic ellipsometry was performed using a J.A. Woollam M-2000 ellipsometer, while fitting was done using the CompleteEASE software. Film thickness was measured on p-type Si(100) using X-Ray Reflectivity (XRR). Both XRR and X-Ray Diffraction (XRD) were carried out using a Bruker D8 diffractometer using Cu Kα radiation. X-Ray Photoelectron spectroscopy (XPS) was performed using a Thermo Scientific Theta Probe XPS using Al Kα radiation. Calibration of the XPS spectra was performed using the C 1s position at 284.6 eV. Elastic Recoil Detection[26] (ERD) was carried out using a 8.0 MeV $^{35}Cl^{4+}$ beam, with a sample tilt of 15° and a scatter angle of 40.5°.

Electrochemical testing with planar electrodes. Planar electrochemical tests were performed in a argon filled glovebox in which the water and oxygen levels are kept below 1 ppm. A PTFE body is filled with electrolyte (1 M $LiClO_4$ in propylene carbonate (99.7%, Sigma-Aldrich)) and clamped against the working electrode (material of interest, with the coating pointing towards the electrolyte). The total surface area of the working electrode that is exposed to the liquid electrolyte is 1.05 cm^2. Li-strips (99.9%, Sigma-Aldrich) were used as both counter and reference electrodes. For testing the electronic conductivity, a solution of 10 mM ferrocene (98%, Sigma-Aldrich) and 100 mM Tetrabutylammonium perchlorate (≥98%, Sigma-Aldrich) in propylene carbonate was made. Platinum wire (99.9%, Sigma-Aldrich) was used as the counter electrode. Measurements were carried out using either a home-built[27] or a commercial (Metrohm Autolab PGSTAT702) potentiostat/galvanostat.

Electrochemical testing with porous electrode. $Li(Ni_{0.6}Mn_{0.2}Co_{0.2})O_2$ (commercial product),

Carbon black (IMERYS Super C45), PVDF (SOLEF 5130-SOLVAY) and NMP (≥99.8%, LSI grade, Carl Roth GmbH) were used to prepare slurries for the cathode electrode. The slurries contained 92 wt% of NMC622, 3.55 wt% of carbon black and 4.45 wt% of PVDF. To ensure a homogenous mixing of all the components, a sequential use of ultrasonic bath and planetary mixer was chosen. The whole mixing process took 20 minutes when three sets of 4 minutes planetary mixing were accomplished and each step followed by a 4 minutes sonication. Cathode electrodes were made by casting the slurry on the current collector (aluminum foil) using a doctor blade. Then, electrodes were dried at 80°C for 10h. After this step, electrodes were calendared, punched into 15 mm disks and dried thoroughly at 110°C under vacuum overnight. The ratio of solid to solvent in the slurry, the height of the doctor blade and the degree of calendaring were adjusted in order to obtain electrodes with desirable thicknesses and porosities. Standard 2325 coin-cells were assembled in an argon-atmosphere glove box. Lithium foil was used as the counter electrode and Celgard-2400 was used as the separator. The electrolyte was 1M $LiPF_6$ in EC:EMC (3:7 w/w). All cells were tested using the Bio-Logic BSC-815 cycler. The cells were at rest for 24h after assembly and then charged-discharged at C/10 for three cycles as the formation step. The rate capability and cyclability tests were performed between 3.0 V and 4.3 V vs Li at room temperature.

Results and dicussion

Deposition of N-doped titanium phosphate

Plasma polymerisation. From earlier work, it is known that when TMP[28] and/or DEPA[9] are pulsed as a plasma, polymerisation reactions can occur. This means that, when pulsed below a certain threshold temperature, non-saturating CVD growth will be observed due to polymerisation of phosphate esters. Only at elevated temperatures, these polymerisation reactions become inhibited and the precursors show self-limiting growth. For DEPA*, this effect is demonstrated in figure 1, where PE-CVD polymerisation rate of DEPA* decreases with increasing substrate temperature. At temperatures around approximately 325°C, the

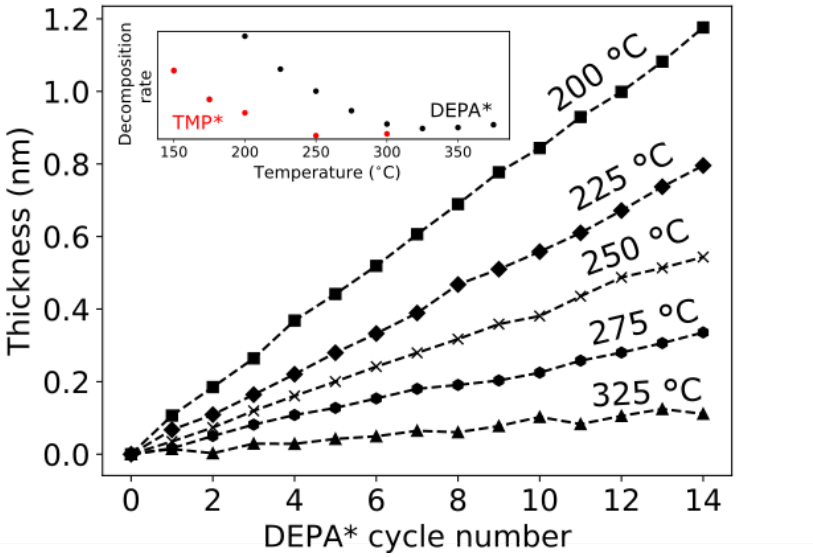

Figure 1: In-situ monitoring of thin film growth, resulting from the surface polymerisation reactions of the DEPA molecule. Each cycle consists of a 2 second pulse of DEPA* at a specific substrate temperature. Insert shows the decomposition rate (amount of growth per second of precursor exposure) of DEPA* and TMP*[28] at different substrate temperatures.

polymerisation reactions exhibit saturation behaviour, suggesting that self-limiting ALD reactions using DEPA* (and TMP*[28]) as reagent becomes possible.

Trimethyl phosphate. Fast PE-ALD deposition of undoped Ti-phosphate has already been investigated by Dobbelaere et al.[16] In his work it was shown that saturated growth of a Ti-phospate can be achieved by combining TMP* with TTIP at a sufficiently high substrate temperature. An oxygen plasma could further be incorporated after the TMP* to assist in removing carbon contamination from the thin film.

In an attempt to achieve nitrogen doping of the Ti-phosphate, the oxygen plasma in the work of Dobbelaere et al. was replaced in this work by a nitrogen plasma at a substrate temperature of 300° (figure 2). This temperature was chosen as the metal phosphate process using oxygen plasma showed saturation at this substrate temperature. Saturation of the new TMP* - N_2* - TTIP process was then studied using in-situ ellipsometry. For this saturation

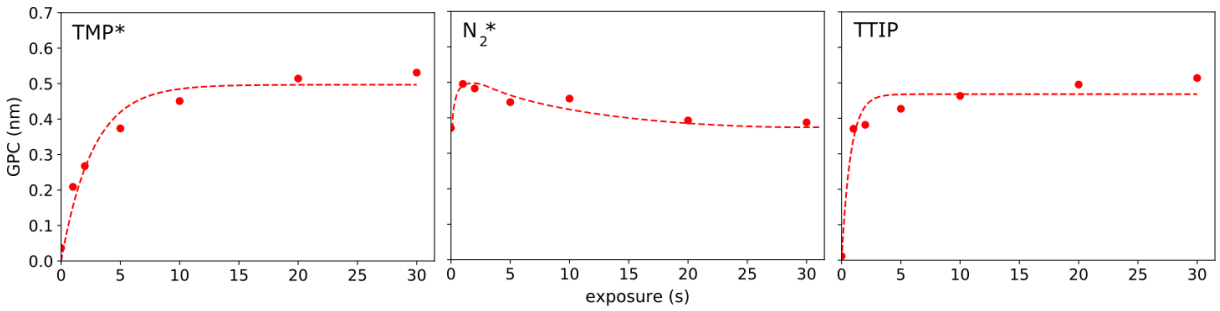

Figure 2: Growth per cycle as a function of precursor pulse time for TMP*, N_2* and TTIP in a TMP*-N_2*-TTIP PE-ALD process at 300°C. The GPC values were extracted from in-situ thickness measurements recorded by ellipsometry and fitted using a Cauchy model. An exponential was fitted for the saturation of DEPA* and TMA, while a guide to the eye was used for N_2*.

experiment, the exposure of two of the three process steps was kept constant at 10s, while the exposure for the other process step was varied.

Saturation for all process steps is found around 0.4 nm/cycle. For TMP* and TTIP, a curve of the shape (1 - e^{-x}) was fitted, while a guide to the eye was used for the nitrogen plasma. For the latter, the GPC first shows to increase at low plasma exposure, while it decreases at higher exposure. This was also seen in our previous work on N-doping of Al-phosphate[9], and was thought to be caused by the removal of carbon groups at initial exposure (activating the surface) and a densification of the film at increasing exposure.

Diethyl phosphoramidate. As DEPA can be used as a 'dual-source' precursor (incorporation of phosphorus and nitrogen), it could allow for higher nitrogen doping, or the elimination of the intermediate nitrogen plasma. Only the growth of the complete DEPA* - N_2* - TTIP process will be discussed here, as the Ti-phosphate resulting from the simplified DEPA* - TTIP process suffers from a high carbon contamination (as will be discussed below).

The ALD behaviour of the second process that is proposed to achieve N-doped Ti-phosphate (i.e. DEPA* - N_2* - TTIP) was then investigated by studying the saturation of each process

step (figure 3). During these measurements, the exposure of each precursor was fixed at 16s, 10s and 15s for respectively DEPA*, N_2* and TTIP. Similar to the previous process, two out of three process steps were kept constant at the given exposure, while the exposure of the third precursor was varied.

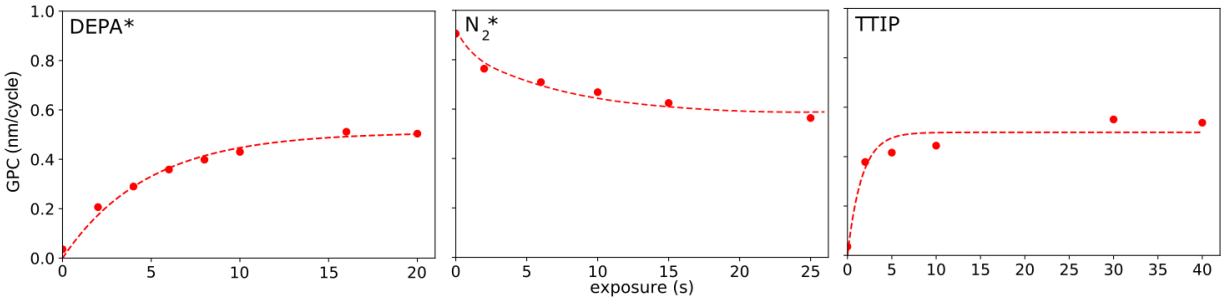

Figure 3: Growth per cycle as a function of precursor pulse time for DEPA*, N_2* and TTIP in a DEPA*-N_2*-TTIP PE-ALD process at 300°C. The GPC values were extracted from in-situ thickness measurements recorded by ellipsometry and fitted using a Cauchy model. An exponential was fitted for the saturation of DEPA* and TMA, while a guide to the eye was used for N_2*.

Again, a curve of the shape (1 - e^{-x}) was fitted to DEPA* and TTIP, while the nitrogen plasma line is a guide for the eye. Both DEPA* and TTIP also show the initial increase with a saturated GPC at high exposures, while the GPC directly decreases as a function of N_2* exposure. This could again be related to densification of the deposited film during the nitrogen plasma step.

From figure 4, it can be seen that, when combining 30s DEPA* with 15s N_2 and 15s TTIP, the GPC changes with varying substrate temperature in a similar way as when only DEPA* is pulsed. However, while a thin film resulting from DEPA* pulses barely grows on its own at high temperatures, the complete process does have a relatively high GPC. Due to the onset of TTIP decomposition at elevated substrate temperatures[29], and the saturation of all three precursors at 300°C, this substrate temperature was chosen for all further depositions. It is found that, at this temperature, a GPC of approximately 0.6 nm/cycle is obtained. This is a

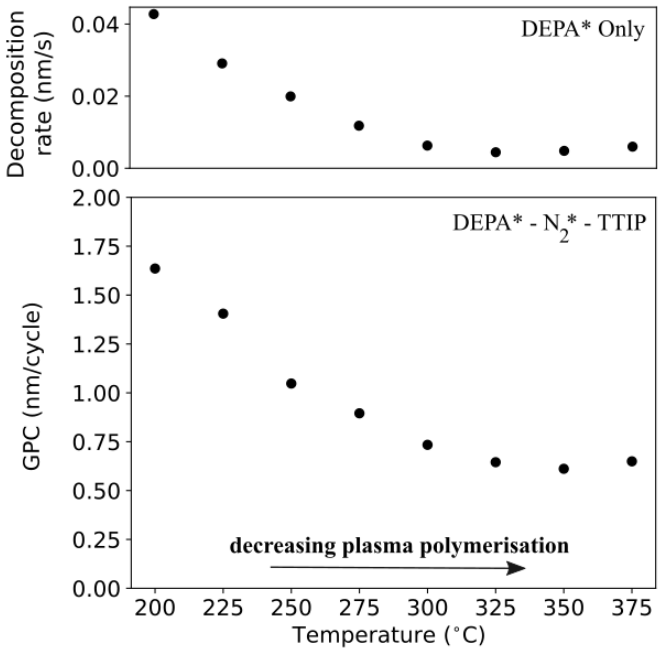

Figure 4: Growth of a thin film resulting from (top) only DEPA* pulses and (bottom) the complete DEPA*-N_2*-TTIP, as a function of the substrate temperature. The growth for only DEPA* is characterized by the growth per second of plasma exposure, while the growth in the complete process is characterized by the thickness resulting from one full process cycle.

similar growth rate as undoped Ti-phosphate, but slightly higher than the first process that was proposed for nitrogen doping (i.e. TMP* - N_2* - TTIP). This could be due to a higher amount of triply coordinated nitrogen (nitrogen bound to 3 phosphorus atoms instead of 2) for the process using DEPA* as compared to the process using TMP* (as will be discussed below).

Thin film characterisation

Film composition. To study the effect of the different process steps on the thin film composition, XPS was performed on a series of samples deposited using different processes. The bulk concentrations resulting from different Ti-phosphate deposition processes can be found in table 1. The process of the undoped phosphate is included for reference.

Different variations of the intermediate plasma step were investigated (i.e. O_2*, O_2* - N_2*, N_2* - O_2* and N_2*) for both TMP* based processes and DEPA* processes. It is seen that a nitrogen plasma can be used to incorporate nitrogen for processes based on both TMP* and DEPA*, but a subsequent oxygen plasma step (i.e. N_2* - O_2*) removes this nitrogen completely. If the nitrogen plasma is pulsed directly after the oxygen plasma (i.e. O_2* - N_2*), a small amount of nitrogen can be incorporated in the film, but the highest doping levels (approximately 5.5 at.% for TMP* - N_2* - TTIP and 10 at.% for DEPA* - N_2* - TTIP) can be achieved by completely removing the oxygen plasma step from the deposition process. In these optimized processes, the nitrogen plasma also acts as an efficient process step for carbon removal. This result is in line with our previous work on nitrogen doping of Al-phosphate[9], showing that the effect of the different intermediate plasma steps does not seem to depend heavily on the metal precursor.

Table 1: Atomic concentrations of N-doped Ti-phosphate with different intermediate plasma, measured with XPS. Concentrations labelled with '-' were below the detection limit

Deposition process	**C (at.%)**	**N (at.%)**	**P (at.%)**	**O (at.%)**	**Ti (at.%)**
TMP*-O_2*-TTIP	-	-	27.1	61.8	11.1
TMP*-O_2*-N_2*-TTIP	-	1.0	28.4	61.7	8.9
TMP*-N_2*-O_2*-TTIP	-	-	26.0	62.0	12.0
TMP*-N_2*-TTIP	-	5.5	30.0	53.0	11.5
DEPA*-TTIP	15.0	2.5	33.5	42.0	7.0
DEPA*-O_2*-TTIP	-	-	27.3	61.8	10.9
DEPA*-O_2*-N_2*-TTIP	-	1.0	27.5	60.0	11.5
DEPA*-N_2*-O_2*-TTIP	-	-	26.6	62.8	10.6
DEPA*-N_2*-TTIP	3.0	10.0	42.0	35.0	10.0

For the processes based on DEPA*, it also has to be noted that the nitrogen plasma can be left out in an attempt to achieve a simplified deposition process for nitrogen doped (2.5 at.%)

Ti-phosphate, but this leads to a high level of carbon contamination (15 at.%). When only an intermediate oxygen plasma is used in these DEPA*-based processes, the composition is close to the film resulting from the original TMP*-O_2*-TTIP, with a similar GPC of 0.7 nm/cycle. This was also found in the previous work on N-doped Al-phosphate[9], confirming that the deposition of undoped metal phosphates via PE-ALD is not restricted to the use of TMP as the phosphorus source.

Table 2: Atomic concentrations of N-doped Ti-phosphate, measured with ERD.

Deposition process	**C (at.%)**	**N (at.%)**	**P (at.%)**	**O (at.%)**	**Ti (at.%)**
TMP*-O_2*-TTIP[16]	/	/	20.0	65.0	12.0
TMP*-N_2*-TTIP	0.4	6.0	21.9	56.2	9.7
DEPA*-N_2*-TTIP	2.2	8.6	25.2	47.6	7.6

To get a more reliable composition, elastic recoil detection[26] (ERD) was used for 60 nm thin films resulting from the TMP*-N_2*-TTIP and the DEPA*-N_2*-TTIP processes. The ERD

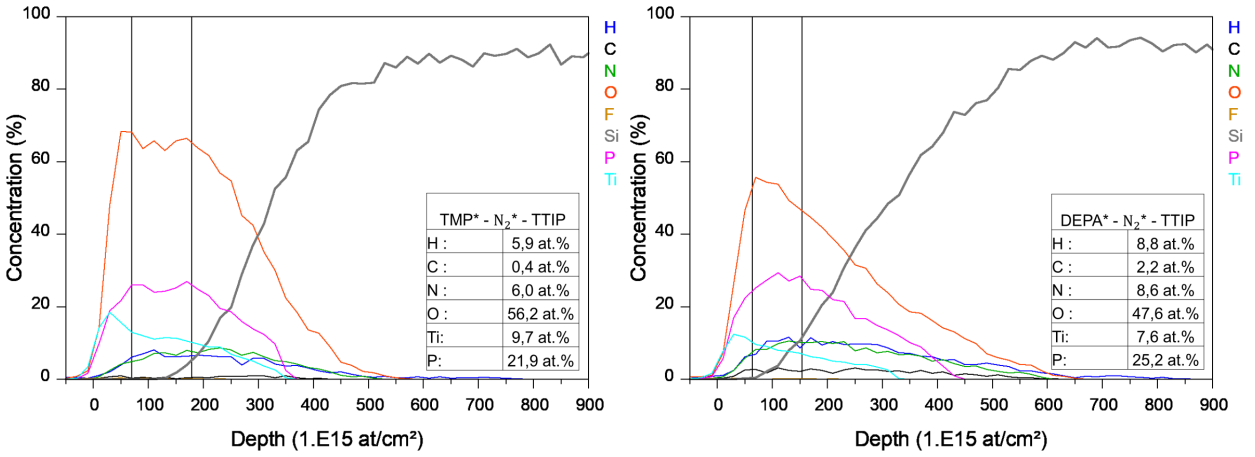

Figure 5: ERD depth profile for N-doped Ti-phospate, using (left) TMP as phosphorus precursor and (right) DEPA as source.

depth profile and composition for both processes (and the undoped process for reference) are shown in figure 5 and table 2. From this it can be seen that the 'dual-source' DEPA

precursor allows for a nitrogen level of 8.6 at.%, while the process using TMP allows for only 6 at.% of nitrogen. For studying the effect of nitrogen doping on the electrochemical performance of Ti-phosphate (see later), undoped Ti-phosphate will be compared to the film resulting from the DEPA*-N_2*-TTIP process, as it allows for the highest growth rate and the highest nitrogen content.

From these compositions, it is now clear that nitrogen doping can be obtained using a dual-source precursor (DEPA*) and/or a nitrogen plasma, but it is not yet known how this nitrogen is built into the thin film. As this chemical structure can help to get a better understanding on the electrochemical influence of nitrogen, the peak position and peak shape obtained from the XPS measurements were studied in more detail.

Chemical structure of N-doped Ti-phosphate. Based on the XPS results in figure 6, the effect of each precursor can be evaluated. First, the TMP* - N_2* - TTIP process will be studied to get a better understanding on how a nitrogen plasma alters the phosphate structure and allows for in-situ nitrogen doping. When looking at the shape of the O1s peak, it can be seen that it consists of two regions. At low energy (531.3 eV) a P-O peak is found, close to the reported value for Ti-phosphate. At higher binding energy (533.3 eV) a P-O-P bond is expected, similar to what is typically found LiPON[31]. The percentage of P-O-P bonds decreases from 11 % of the total O 1s area when using an oxygen plasma (i.e. TMP* - O_2* - TTIP) to 7 % when using a nitrogen plasma (i.e. TMP* - N_2* - TTIP). This means that the ratio of bridging oxygen/non-bridging oxygen decreases upon nitrogen doping, which has been proven to be of importance for improved electrochemical behaviour[32]. The N1s peak can be split in two regions, similar to what is found in LiPON studies[31,33,34]. A triply coordinated nitrogen bond (-N<) is found at 399.2 eV, while also a double coordinated bond (-N=) is present with a peak energy of 397.7 eV. As the latter one is the most intense, it can be concluded that the nitrogen plasma prefers to incorporate doubly coordinated nitrogen

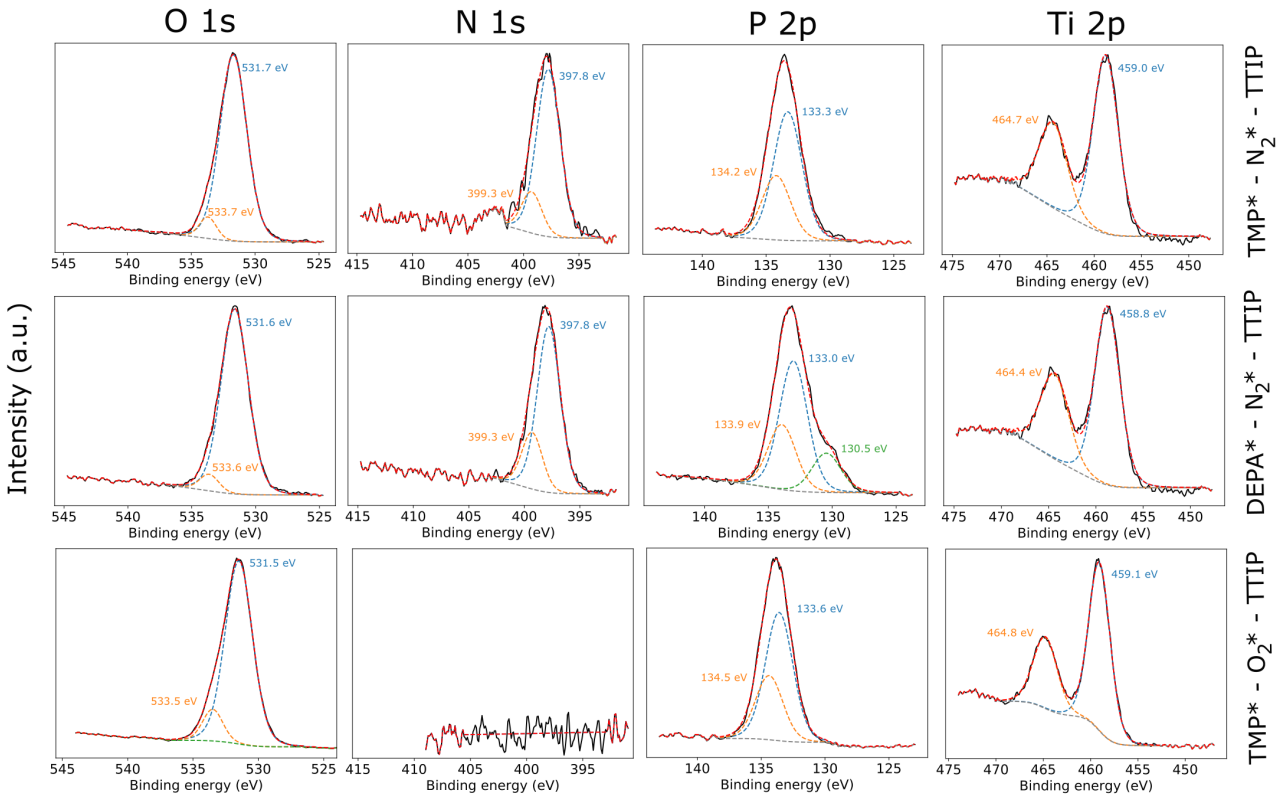

Figure 6: XPS spectra of the O 1s, N 1s, P 2p and Ti 2p peaks. For all the peaks, at least two components were used to fit the spectrum for both N-doped Ti-phosphate deposited with TMP* and DEPA* and the undoped Ti-phosphate for reference. The peak position of each component is also shown.

in the phosphate esters, similar to what is seen in the work of Kozen et al[31]. The P2p peak has a binding energy of 133.6 eV (deconvoluted as P $2p_{3/2}$ at 133.3 eV and P $2p_{1/2}$ 134.2 eV), which is slightly lower than undoped phosphate. This is in agreement with the more nitrogen rich environment[35]. The Ti 2p peaks at 464.7 eV ($2p_{3/2}$) and 459.0 eV ($2p_{1/2}$) did not shift a lot upon nitrogen doping (464.8 eV and 459.1 eV respectively for undoped Ti-phosphate), showing that the environment of these atoms did not change dramatically.

Now that the effect of the nitrogen plasma is clear, the more nitrogen rich DEPA* - N_2* - TTIP process can be studied in detail. The first important difference by changing from TMP to DEPA can be found in the O 1s peak, where the P-O-P component further decreases from

7% to 6%. This agrees with the overall increase of the nitrogen content. Both Ti 2p and P 2p peaks do not shift considerably, but an extra phosphorus component arises when DEPA is used as the phosphorus source. Although it is not clear what the origin of this peak is, the position is close to elemental phosphorus (P $2p_{3/2}$ at 130.2 eV). A possible explanation could be breaking of the P-NH_2 bonds in two DEPA molecules, which are then linked through a P-P bond, which could partially explain a lower than 1 P/N-ratio, which is observed in ERD. The fact that this extra peak only appeared after sputtering away the surface layer further supports this (as this bond is easily oxidisable).

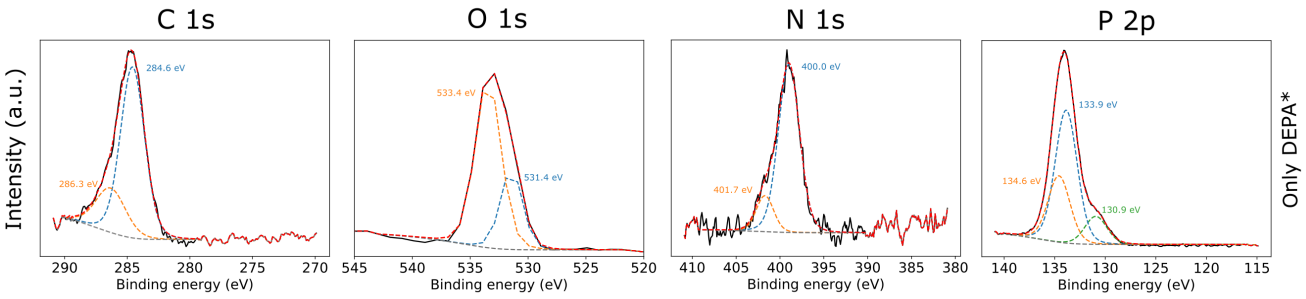

Figure 7: XPS study of a thin film grown by decomposition of DEPA* at 150°C. Each peak was fitted using at least two components, of which the peak position is labelled next to the component.

The N 1s peak did not shift by going from TMP* to DEPA*. However, the contribution of the triply coordinated nitrogen increased from 14% of the total N 1s area to 23%. To understand this increase, the DEPA plasma polymerisation can be studied in more detail. As films grown at a temperature of 150°C result from the surface polymerisation of DEPA plasma species, this low temperature PE-CVD film can provide clues on the composition and chemical nature of the plasma constituents (see figure S1). Using XPS (figure 7) to study the N 1s peak reveals that there are two types of nitrogen built into the film deposited by DEPA* polymerisation. The small peak at 401.7 eV is close to the binding energy that is typically found in P-NH_2 bonds[36]. This means that a small part of the amine groups did not undergo any reaction. The biggest contribution is however the peak at 399 eV, arising from

triply coordinated nitrogen (>N -)[31]. From this it can be concluded that most amine groups do participate in the reaction mechanism, and that nitrogen from DEPA* is preferably triply coordinated. For that reason, the contribution of triply coordinated nitrogen increases when going from TMP* - N_2* - TTIP to DEPA* - N_2* - TTIP.

For the other elements, also at least two components were used to fit each peak. For C 1s, a peak related to C-C bonds was found at a binding energy of 284.6 eV, while the peak at 286.3 eV is thought to be due to C-O bonds from the diethyl group. Most oxygen in the film is found in a P-O-P bond (the largest contribution to the O 1s peak is found at 533.4 eV). This is to be expected, as this is one of the main bonds through which the phosphate esters can be linked. It is only at elevated temperatures, and with the incorporation of a metal precursor, that the component around 531 eV can become dominant. In the P 2p peak, the extra shoulder at low binding energies is again visible, showing that this specific bond that was observed in the DEPA* - N_2* - TTIP process is indeed formed during the plasma activation of DEPA.

Film crystallinity. Using XRD, it can be seen that N-doped Ti-phosphate (using TMP*) is amorphous as deposited. However, upon annealing up to 950°C in a He-atmosphere, peaks that can be linked to crystalline TiP_2O_7 (JCPDS #00-038-1468)[30] appear. Like the thin films that are deposited with TMP*, the films deposited with DEPA* are also amorphous. Upon annealing, the same peaks arise showing the similarities between the films deposited with TMP* and DEPA*.

Electrochemical characterisation

Next, the electrochemical properties of (N-doped) Ti-phosphate were studied. In these tests, thin films resulting from the TMP* - O_2* - TTIP process were compared to thin films resulting from DEPA* - N^*_2 - TTIP (as these contained the highest nitrogen levels and the lowest

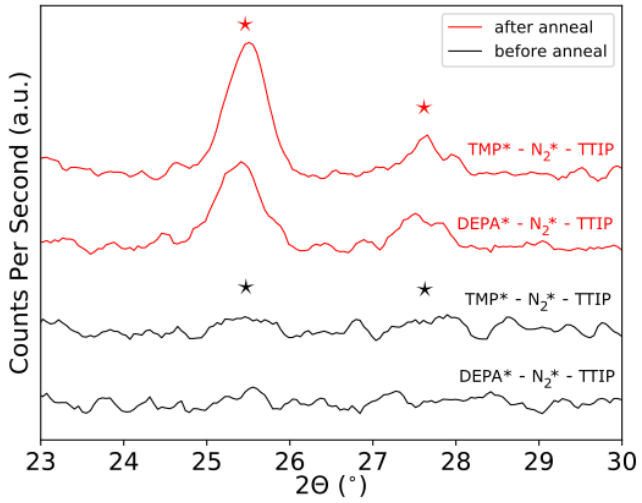

Figure 8: XRD data before and after annealing up to 950°C in He-atmosphere. The stars denote peak positions of crystalline TiP_2O_7 (JCPDS #00-038-1468)[30].

amount of P-O-P bonds). To study the ionic and electronic conductivity of Ti-phosphate, and how this is altered by incorporating nitrogen, both coatings were first deposited on a TiO_2 electrode (to study ionic conductivity) and an electronically conductive TiN film (to study electronic conductivity). These films were then deposited onto a NMC powder to study the effect of the coating in powder-based electrodes.

Ionic conductivity on TiO_2. To get an idea of the ionic conductivity of Ti-phosphate, and how it is affected by nitrogen doping, (N-doped) Ti-phosphate is deposited on a 40 nm TiO_2 electrode. The cylic voltammogram of the (un)coated electrode systems is shown in figure S2.

By first measuring the capacity of the (un)coated electrode at different current densities, it can be seen how much the coating is blocking diffusion of Li-ions into the electrode. In figure 9, the charging capacities of different coated electrodes are shown at different C-rates. Apart from the coatings from this work, also a 1 nm Al_2O_3 coating[8] and a 1 nm Al-phosphate coating[9] are shown for reference (from our earlier work). From the reference data it can now be seen that, although these materials have been reported to be excellent coating materials,

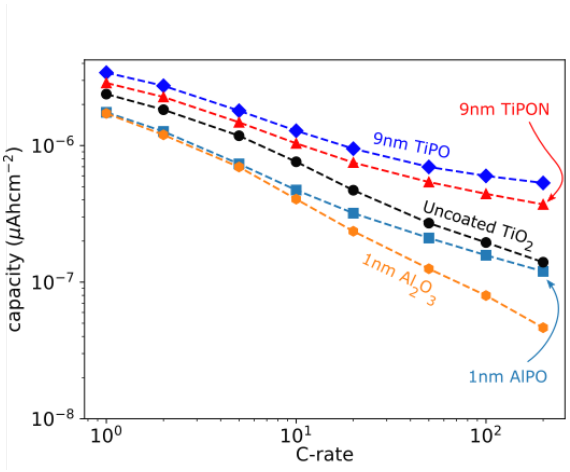

Figure 9: Lithiation capacity of (un)coated TiO_2 using different coating materials. Capacities using Al_2O_3 (1 nm)[8] and Al-phosphate (1 nm, denoted as AlPO)[9] as coating are shown as reference. A coating thickness of approximately 9 nm for both Ti-phosphates. TiPO is used to refer to undoped Ti-phosphate, while TiPON is used for N-doped Ti-phosphate.

a 1 nm layer of inactive material already leads to a decrease in the rate capability of the electrode. It is thus important to know that these coatings require sub-nanometer control on the coating thickness in order minimise this effect. On the other hand, depositing 9 nm of the (un)doped Ti-phosphate on the electrode shows to increase the capacity at every C-rate. The increase in capacity is thought to be due to the phosphate, which is in itself also electrochemically active in the potential range that was used (between 1.0 V and 3.0 V vs. Li^+/Li). The fact that the capacity is slightly lower after nitrogen doping of the coating could mean that the phosphate becomes less active after nitrogen doping (hence less additional capacity is measured), although this was not studied further. The overall decrease in capacity of both Ti-phosphate coated systems with increasing C-rate is however very similar to the uncoated electrode, meaning that the rate limiting factor is not the coating (as is typically the case with inert coatings), but the electrode itself. This shows that, even for a coating that is significantly thicker (9 nm) than the inactive reference coatings (1 nm), the Li-ions are still able to easily diffuse through the coating. The same conclusion can be made from the capacities measured during discharging, as is shown in figure S2.

To get a more detailed view on the ionic resistance of the coating, and how this is affected by nitrogen doping, the peak current and peak potential of the cyclic voltammogram can be measured at different scan rates. Based on these measurements, the shift in peak current and peak potential with increasing scan rate can be a way of determining the ionic resistance of the electrochemical system[9]. The relation between peak current and peak potential can thus be used to calculate the total ionic resistance of both coated and uncoated systems (by means of the inverse slope of the linear fit), and the difference between both values (arising from the so called IR-drop over the coating) is then the coating resistance. When the coating thickness, and electrode area are then also taken into account, a transversal ionic conductivity can be calculated. This is not the actual ionic conductivity (as this is not a bulk material), but it does provide a way to compare the ionic transparency of the coating of interest.

From these measurements (figure 10), an effective transversal ionic conductivity of (2.3 $\pm$ 1.7)$*10^{-7}$ mS/cm and (1.6 $\pm$ 1.0)$*10^{-7}$ mS/cm was found for respectively undoped and

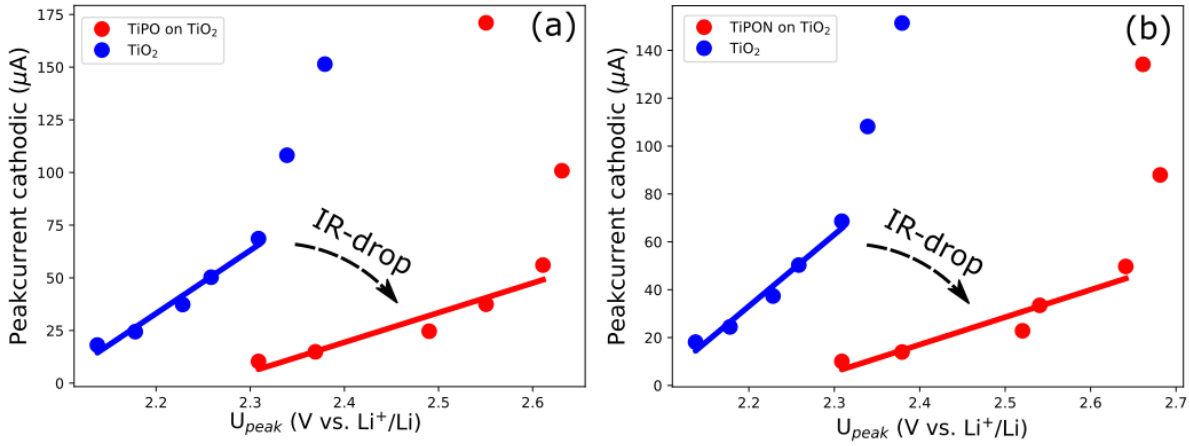

Figure 10: Calculation of the resistance for both approximately (a) 9 nm of Ti-phosphate and (b) 9 nm of N-doped Ti-phosphate. The measured resistances are (7.1 $\pm$ 2.3) kΩ for the electrode coated with undoped Ti-phosphate (denoted as TiPO) and (8.7 $\pm$ 2.9) kΩ for the electrode coated with N-doped Ti-phosphate (denoted as TiPON). The resistance of the uncoated TiO_2 electrode is (3.3 $\pm$ 0.6) kΩ.

N-doped Ti-phosphate. Nitrogen doping seems to decrease the ionic transparency of the coating, but no conclusive answer can be found due to the large error margins. It also has to be noted that the Ti-phosphate is also electrochemically active in the potential window that was used, so the results might not be exactly the same on an electrode which operates outside of the potential window in which Ti-phosphate is active. Nevertheless, it does already give an idea on the possible impact of nitrogen doping.

Electronic conductivity on TiN. In using a redox couple based on the exchange of an electron instead of a Li-ion, the effect of nitrogen doping on the electronic conductivity can be made. In this work, this was done by using platinum as the reference and counter electrode, coated TiN as working electrode and a ferrocene electrolyte to make use of the reversible ferrocene redox couple. From the cyclic voltammogram of this ferrocene system, we can then again extract the peak current and peak potential at different scan rates to obtain a measure for the electronic conductivity.

From these measurements (see figure S3) an effective transversal electronic conductivity of $(1.1 \pm 0.1)*10^{-7}$ mS/cm and $(3.7 \pm 0.3)*10^{-7}$ mS/cm is found for respectively undoped and N-doped Ti-phosphate. This shows that the electronic conductivity of the coating can be increased with nitrogen doping.

(N-doped) Ti-phosphate as a functional coating for powder-based electrodes. Before looking at the electrochemical effect of these Ti-phosphate coatings on powder-based electrodes, approximately 20 nm of N-doped Ti-phosphate was deposited on lithium nickel manganese cobalt oxide (NMC) powder. The surface of the particle was then studied using SEM/EDX to see if deposition on the complex powder surface is possible. In figure 11 it can be seen that, although on SEM we do not see any sign of a non-conformal shell, phosphorus and titanium are present at the surface of the particle. This shows that the coating can be

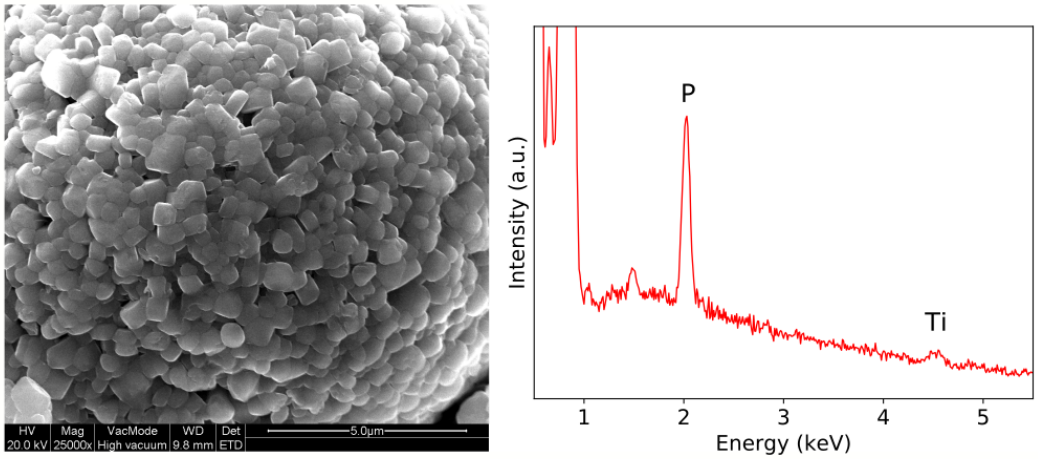

Figure 11: 20 nm of N-doped titanium phosphate on NMC powder, studied with (left) SEM and (right) EDX. The EDX spectrum was measured for 500s with a 10 kV acceleration voltage.

deposited on the NMC particle surface.

A coating of approximately 2 nm of (un)doped Ti-phosphate (resulting from 3 cycles of the respective deposition processes) was then deposited on NMC for electrochemical characterisation. First, the specific energy density of the (un)coated electrodes was measured at different C-rates (C/5, C/2, 1C, 2C and 5C), as shown in figure 12a. It can be seen that, in contrast to a 1 nm Al-phosphate coating[9], the rate capability of the electrode has significantly improved due to the coating. Although minor difference in ionic and electronic conductivity of the coating were measured (on planar electrodes) after nitrogen doping, there does not seem to be a big difference in their electrochemical performance as a NMC coating. The difference might however be more pronounced with different electrode formulations (see supporting information). Overall, the electrochemically active nature of Ti-phosphate thus enables an enhancement of the rate capability, without the need for a high control (at the sub-nanometer level) on the coating thickness.

The cyclability of the (un)coated electrodes is shown in figure 12b. It can be seen that, while

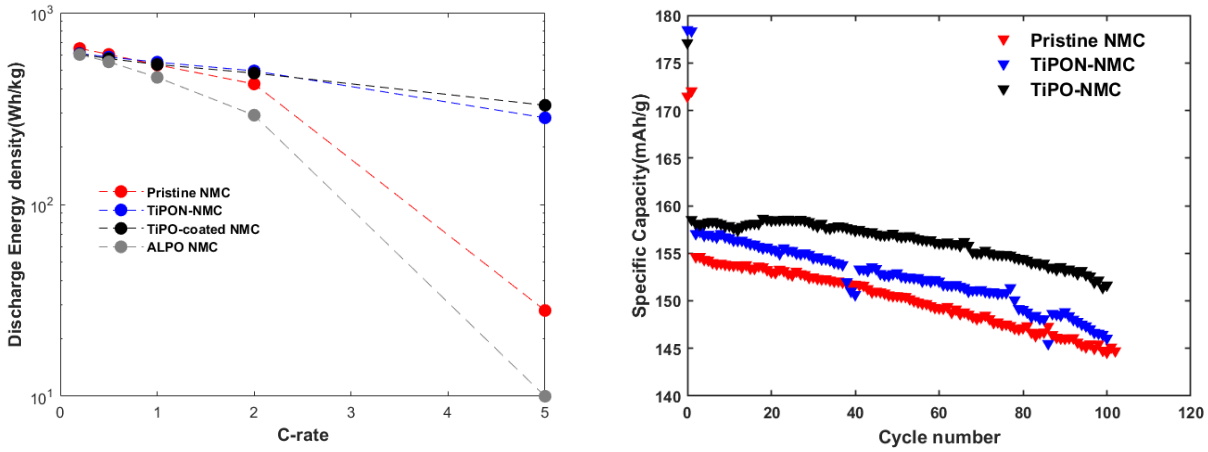

(a) (b)

Figure 12: (a) Energy density of (un)coated NMC powder electrodes at different C-rates and (b) the capacity evolution during 100 cycles at a rate of 1C. The loading of active material is 13 mg/cm^2. Data for the electrode coated with 1 nm of Al-phosphate has been used from our previous work[9].

N-doped Ti-phosphate does not harm the good cyclability of NMC, undoped Ti-phosphate seems to improve it even more. Phosphates are interesting materials as protective coatings, as the strong P-O bonds can increase the thermal stability of the electrode, besides possibly limiting other parasitic reactions. This means that the differences (also for NMC coated with N-doped Ti-phosphate versus uncoated NMC) could be more visible at elevated temperatures. This was however not studied here (Currently tests are running on this). The fact that we do see an improvement in capacity retention for electrodes coated with undoped Ti-phosphate, and not for N-doped Ti-phosphate coated electrodes could be due to a difference in coating nature, or due to a less conformal deposition of the latter.

From this work, it can thus be seen that the use of an electrochemically active coating material is beneficial towards increasing the electrodes rate capability, without harming the good cycling stability of NMC. A possible explanation for this improvement could be that the coating is now taking up a functional role for the transportation of Li-ions and electrons throughout the electrode sheet. Instead of coatings that impose a physical barrier between

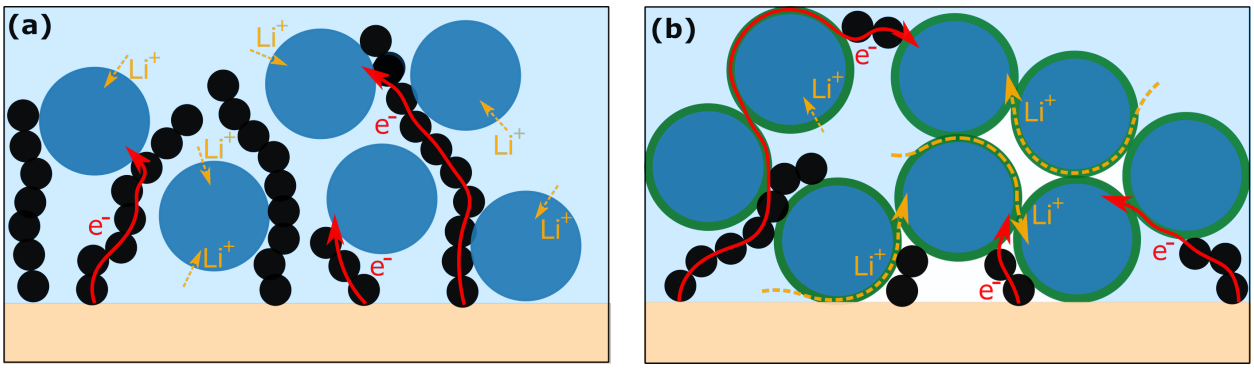

Figure 13: Schematic of the composite electrode on the current collector (pale orange): Active particles (blue, with a green ring if coated), carbon black particles (black) and the electrolyte (light blue). (a) An electrode formulation in which almost no isolated particles are present, but suffers from a low amount of active material per unit of volume. (b) If there is a decrease in the amount of carbon black and the porosity (depicted by white voids without electrolyte), the coating can be used to enhance particle accessibility. This allows for more active material to be present in the same volume.

the electrode particle and the electrolyte (decreasing the ionic and/or electronic conductivity of the electrode), the coatings in this work might be used as a local conductive network, enhancing the mobility of Li-ions and electrons. This is important, as it would allow us to store more energy in a smaller volume by for example decreasing the amount of carbon black or decrease the electrode porosity, as explained in figure 13. In the case of uncoated particles, optimal accessibility of each particle to both Li-ions and electrons is obtained in a formulation with a high amount of carbon black and high electrode porosity (depicted in 13a). Unfortunately, this severely limits the amount of energy (i.e. the amount of electrode particles) that can be stored per unit of volume, as decreasing the amount of carbon black and/or the porosity will make some particles completely isolated from the electron/Li-ion source. If the electrode particles are now coated with a material that has a sufficiently good ionic/electronic conductivity, the coating could be used as a local pathway to reach the isolated areas (depicted in 13b). This means that the coating could make isolated particles easier to be reached, allowing for an increase in the amount of active material per unit of volume without decreasing the overall ionic and electronic conductivity of the electrode sheet. Making the transition (using a fixed electrode formulation) from an inert coating

(or no coating) to for example the coatings proposed in this work could thus allow for the overall ionic/electronic conductivity to be increased, resulting in an improvement of the rate capability (as seen in figure 12). The effect of a decrease in contact points between the carbon black and the particles on the one hand, and a decrease in the electrode porosity on the other hand is further discussed in the supporting information.

Conclusion

Nitrogen doped Ti-phosphate has been successfully deposited using two different PE-ALD processes. The first approach was based on an existing process for undoped Ti-phosphate, in which the oxygen plasma was replaced by a nitrogen plasma (i.e. TMP* - N^*_2 - TTIP). This allowed for the deposition of a thin film with a GPC of 0.4 nm/cycle, and a nitrogen doping level of 6 at.%. Replacing TMP* by the dual-source precursor DEPA* allowed for a faster deposition (0.6 nm/cycle, similar to the deposition rate of undoped Ti-phosphate) and a higher nitrogen level of 8.6 at.%. Both nitrogen doped films were amorphous as deposited, but could be crystallized into TiP_2O_7 upon annealing in He atmosphere. To understand the effect of nitrogen on the electrochemical performance of the Ti-phosphate, the most nitrogen rich phosphate (resulting from DEPA* - N^*_2 - TTIP) was compared to the undoped phosphate (resulting from TMP* - O^*_2 - TTIP). From planar tests, it could be seen that nitrogen doping slightly decreased the effective transversal ionic conductivity from (2.3 $\pm$ 1.7)$*10^{-7}$ mS/cm to (1.6 $\pm$ 1.0)$*10^{-7}$ mS/cm, while the effective electronic conductivity increased from (1.1 $\pm$ 0.1)$*10^{-7}$ mS/cm to (3.7 $\pm$ 0.3)$*10^{-7}$ mS/cm. A coating of 2 nm on NMC powder resulted for both films in a similar increase in rate capability, while the capacity retention of the electrode was not harmed. From this work it can be concluded that our PE-ALD process for nitrogen doping of phosphates can be extended from one phosphate to another, and that these (un)doped coatings show promising features as functional coatings for LIB electrodes.

Acknowledgements

The authors are grateful for financial support to FWO-Vlaanderen and the Special Research Fund BOF of Ghent University (GOA project, Grant No. 01G01513, and SBO XL-Lion, S005017N). M. M. and J.D. acknowledge FWO-Vlaanderen for a post-doctoral fellowship.

References

(1) Chen, Z., Qin, Y., Amine, K., & Sun, Y. (2010). Role of surface coating on cathode materials for lithium-ion batteries. Journal Of Materials Chemistry, 20(36), 7606. doi: 10.1039/c0jm00154f

(2) Wise, A., Ban, C., Weker, J., Misra, S., Cavanagh, A., & Wu, Z. et al. (2015). Effect of Al_2O_3 Coating on Stabilizing $LiNi_{0.4}Mn_{0.4}Co_{0.2}O_2$ Cathodes. Chemistry Of Materials, 27(17), 6146-6154. doi: 10.1021/acs.chemmater.5b02952

(3) J. Cho, T.-J. Kim, J. Kim, M. Noh, and B. Park, "Synthesis, thermal, and electrochemical properties of $AlPO_4$-coated $LiNi_{0.8}Co_{0.1}Mn_{0.1}O_2$ cathode materials for a Li-ion cell", Journal of The Electrochemical Society, vol. 151, no. 11, A1899-A1904, 2004.

(4) J. Cho, Y.-W. Kim, B. Kim, J.-G. Lee, and B. Park, "A breakthrough in the safety of lithium secondary batteries by coating the cathode material with $AlPO_4$ nanoparticles", Angewandte Chemie International Edition, vol. 42, no. 14, pp. 1618-1621, 2003.

(5) Shi, J., Yi, C., & Kim, K. (2010). Improved electrochemical performance of $AlPO_4$-coated $LiMn_{1.5}Ni_{0.5}O_4$ electrode for lithium-ion batteries. Journal Of Power Sources, 195(19), 6860-6866. doi: 10.1016/j.jpowsour.2010.02.063

(6) Liu, D., He, Z., & Liu, X. (2007). Increased cycling stability of $AlPO_4$-coated $LiMn_2O_4$ for lithium ion batteries. Materials Letters, 61(25), 4703-4706. doi: 10.1016/j.matlet.2007.03.012

(7) Cho, J., Kim, T., Kim, C., Lee, J., Kim, Y., & Park, B. (2005). Comparison of Al_2O_3- and $AlPO_4$-coated $LiCoO_2$ cathode materials for a Li-ion cell. Journal Of Power Sources, 146(1-2), 58-64. doi: 10.1016/j.jpowsour.2005.03.118

(8) Mattelaer, F., Vereecken, P., Dendooven, J., & Detavernier, C. (2017). The Influence of Ultrathin Amorphous ALD Alumina and Titania on the Rate Capability of Anatase TiO_2 and $LiMn_2O_4$ Lithium Ion Battery Electrodes. Advanced Materials Interfaces, 4(13), 1601237. doi: 10.1002/admi.201601237

(9) Nog in te vullen

(10) Jung, Y., Cavanagh, A., Riley, L., Kang, S., Dillon, A., & Groner, M. et al. (2010). Ultrathin Direct Atomic Layer Deposition on Composite Electrodes for Highly Durable and Safe Li-Ion Batteries. Advanced Materials, 22(19), 2172-2176. doi: 10.1002/adma.200903951

(11) Xiao, B., Liu, J., Sun, Q., Wang, B., Banis, M., & Zhao, D. et al. (2015). Unravelling the Role of Electrochemically Active $FePO_4$ Coating by Atomic Layer Deposition for Increased High-Voltage Stability of $LiNi_{0.5}Mn_{1.5}O_4$ Cathode Material. Advanced Science, 2(5), 1500022. doi: 10.1002/advs.201500022

(12) Yi, T., Li, Y., Li, X., Pan, J., Zhang, Q., & Zhu, Y. (2017). Enhanced electrochemical property of $FePO_4$-coated $LiNi_{0.5}Mn_{1.5}O_4$ as cathode materials for Li-ion battery. Science Bulletin, 62(14), 1004-1010. doi: 10.1016/j.scib.2017.07.003

(13) Leskelä, M., Niinistö, J., & Ritala, M. (2014). Atomic Layer Deposition. Comprehensive Materials Processing, 101-123. doi: 10.1016/b978-0-08-096532-1.00401-5

(14) Ceder, G. (2010). Opportunities and challenges for first-principles materials design and applications to Li battery materials. MRS Bulletin, 35(9), 693-701. doi: 10.1557/mrs2010.681

(15) Dobbelaere, T., Mattelaer, F., Dendooven, J., Vereecken, P., & Detavernier, C. (2016). Plasma-Enhanced Atomic Layer Deposition of Iron Phosphate as a Positive Electrode for 3D Lithium-Ion Microbatteries. Chemistry Of Materials, 28(10), 3435-3445. doi: 10.1021/acs.chemmater.6b00853

(16) Dobbelaere, T., Mattelaer, F., Roy, A. K., Vereecken, P., & Detavernier, C. (2017). Plasma-enhanced atomic layer deposition of titanium phosphate as an electrode for lithium-ion batteries. Journal of materials chemistry A, 5(1), 330–338

(17) Fang, Y., Zhang, J., Xiao, L., Ai, X., Cao, Y., & Yang, H. (2017). Phosphate Framework Electrode Materials for Sodium Ion Batteries. Advanced Science, 4(5), 1600392. doi: 10.1002/advs.201600392

(18) Dobbelaere, T., Mattelaer, F., Vereecken, P., & Detavernier, C. (2017). Plasma-enhanced atomic layer deposition of vanadium phosphate as a lithium-ion battery electrode material. Journal Of Vacuum Science & Technology A: Vacuum, Surfaces, And Films, 35(4), 041513. doi: 10.1116/1.4987131

(19) Dobbelaere, T., Minjauw, M., Ahmad, T., Vereecken, P., & Detavernier, C. (2016). Plasma-enhanced atomic layer deposition of zinc phosphate. Journal Of Non-Crystalline Solids, 444, 43-48. doi: 10.1016/j.jnoncrysol.2016.04.032

(20) Rongé, J., Dobbelaere, T., Henderick, L., Minjauw, M., Sree, S., & Dendooven, J. et al. (2019). Bifunctional earth-abundant phosphate/phosphide catalysts prepared via atomic layer deposition for electrocatalytic water splitting. Nanoscale Advances, 1(10), 4166-4172. doi: 10.1039/c9na00391f

(21) Attia, A., Wang, Q., Huang, X., & Yang, Y. (2011). Titanium phosphates as positive electrode in lithium-ion batteries: composition, phase purity and electrochemical performance. Journal Of Solid State Electrochemistry, 16(4), 1461-1471. doi: 10.1007/s10008-011-1543-0

(22) Guo, S., Yi, J., Sun, Y., & Zhou, H. (2016). Recent advances in titanium-based electrode materials for stationary sodium-ion batteries. Energy & Environmental Science, 9(10), 2978-3006. doi: 10.1039/c6ee01807f

(23) Voronina, N., Jo, J., Choi, J., Jo, C., Kim, J., & Myung, S. (2019). Nb-Doped titanium phosphate for sodium storage: electrochemical performance and structural insights. Journal Of Materials Chemistry A, 7(10), 5748-5759. doi: 10.1039/c8ta11517f

(24) Deng, S., Verbruggen, S., Lenaerts, S., Martens, J., Van den Berghe, S., & Devloo-Casier, K. et al. (2014). Controllable nitrogen doping in as deposited TiO_2 film and its effect on post deposition annealing. Journal Of Vacuum Science & Technology A: Vacuum, Surfaces, And Films, 32(1), 01A123. doi: 10.1116/1.4847976.

(25) Munoz, F., Duran, A., Pascual, L., Montagne, L., Revel, B., & Rodrigues, A. (2008). Increased electrical conductivity of LiPON glasses produced by ammonolysis. Solid State Ionics, 179(15-16), 574-579. doi: 10.1016/j.ssi.2008.04.004

(26) Meersschaut, J., & Vandervorst, W. (2017). High-throughput ion beam analysis at imec. Nuclear Instruments And Methods In Physics Research Section B: Beam Interactions With Materials And Atoms, 406, 25-29. doi: 10.1016/j.nimb.2017.01.005

(27) Dobbelaere, T., Vereecken, P., & Detavernier, C. (2017). A USB-controlled potentiostat/galvanostat for thin-film battery characterization. Hardwarex, 2, 34-49. doi: 10.1016/j.ohx.2017.08.001

(28) Dobbelaere, T.; Roy, A. K.; Vereecken, P.; Detavernier, C. Atomic Layer Deposition of Aluminum Phosphate Based on the Plasma Polymerization of Trimethyl Phosphate. Chem. Mater. 2014, 26, 6863-6871.

(29) Wu, Y., Bradley, D., & Nix, R. (1993). Studies of titanium dioxide film growth from titanium tetraisopropoxide. Applied Surface Science, 64(1), 21-28. doi: 10.1016/0169-4332(93)90018-7

(30) H. F. McMurdie, M. C. Morris, E. H. Evans, B. Paretzkin, W. Wong-Ng, Y. Zhang and C. R. Hubbard, Powder Diffr., 1987, 2, 52.

(31) Kozen, A., Pearse, A., Lin, C., Noked, M., & Rubloff, G. (2015). Atomic Layer Deposition of the Solid Electrolyte LiPON. Chemistry Of Materials, 27(15), 5324-5331. doi: 10.1021/acs.chemmater.5b01654

(32) Mascaraque, N., Fierro, J., Durán, A., & Muñoz, F. (2013). An interpretation for the increase of ionic conductivity by nitrogen incorporation in LiPON oxynitride glasses. Solid State Ionics, 233, 73-79. doi: 10.1016/j.ssi.2012.12.017

(33) Pearse, A., Schmitt, T., Fuller, E., El-Gabaly, F., Lin, C., & Gerasopoulos, K. et al. (2017). Nanoscale Solid State Batteries Enabled by Thermal Atomic Layer Deposition of a Lithium Polyphosphazene Solid State Electrolyte. Chemistry Of Materials, 29(8), 3740-3753. doi: 10.1021/acs.chemmater.7b00805

(34) Nisula, M., Shindo, Y., Koga, H., & Karppinen, M. (2015). Atomic Layer Deposition of Lithium Phosphorus Oxynitride. Chemistry Of Materials, 27(20), 6987-6993. doi: 10.1021/acs.chemmater.5b02199

(35) Fleutot, B.; Pecquenard, B.; Martinez, H.; Letellier, M.; Levasseur, a. Investigation of the Local Structure of LiPON Thin Films to Better Understand the Role of Nitrogen on Their Performance Solid State Ionics 2011, 186, 29– 36 DOI: 10.1016/j.ssi.2011.01.006

(36) Gaan, S., Sun, G., Hutches, K., & Engelhard, M. (2008). Effect of nitrogen additives on flame retardant action of tributyl phosphate: Phosphorus–nitrogen synergism. Polymer Degradation And Stability, 93(1), 99-108. doi: 10.1016/j.polymdegradstab.2007.10.013